ACS Energy Letters

Subscriber access provided by DGIST

Letter

Electric field mediated selectivity switching of electrochemical CO2 reduction from formate to CO on carbon supported Sn

Mi-Young Lee, Stefan Ringe, Hyungjun Kim, Seoktae Kang, and Youngkook Kwon

ACS Energy Lett., **Just Accepted Manuscript** • DOI: 10.1021/acsenergylett.0c01387 • Publication Date (Web): 12 Aug 2020

Downloaded from pubs.acs.org on August 17, 2020

is published by the American Chemical Society. 1155 Sixteenth Street N.W., Washington, DC 20036

Electric field mediated selectivity switching of electrochemical CO_2 reduction from formate to CO on carbon supported Sn

Mi-Young Lee[†], Stefan Ringe[‡], Hyungjun Kim[§,], Seoktae Kang[†,*], and Youngkook Kwon[⊥,*]*

[†]Department of Civil and Environmental Engineering, Korea Advanced Institute of Science and Technology, 291 Daehak-ro, Yuseong-gu, Daejeon 34141, Republic of Korea

[‡]Department of Energy Science and Engineering, Daegu Gyeongbuk Institute of Science and Technology (DGIST), Daegu 42988, Republic of Korea

[§]Department of Chemistry, Korea Advanced Institute of Science and Technology, 291 Daehak-ro, Yuseong-gu, Daejeon 34141, Republic of Korea

[⊥]School of Energy and Chemical Engineering; and Emergent Hydrogen Technology R&D Center, Ulsan National Institute of Science and Technology, 50 UNIST-gil, Ulsan 44919, Republic of Korea

Corresponding Author

E-mail: linus16@kaist.ac.kr; stkang@kaist.ac.kr; ykwon@unist.ac.kr.

ABSTRACT. Decades of electrochemical CO_2 reduction research have led to established rules about the product selectivity i.e. bare Tin yields formic acid as the main product. Here, we present Sn nanoparticles supported on carbon nanotubes in a hollow fiber (Sn-CHF) which produce CO with 10 times higher selectivity than formate. Density functional theory calculations reveal that a strong interfacial field induced by the carbon support enhances the rate-limiting CO_2 adsorption and thus CO production on Sn nanoparticles whereas the field-insensitive formate and hydrogen production routes were completely suppressed and occurred mainly from carbon sites. Modification of the interfacial electric field via exchange of the electrolyte-containing cation from Li^+ to Cs^+ induces an unprecedented two orders of magnitude change in the CO current, while not changing the other products. This work demonstrates how electrochemical selectivity rules can be modulated by controlling the interfacial field, thus opening up new windows for electrocatalyst design.

TOC GRAPHICS

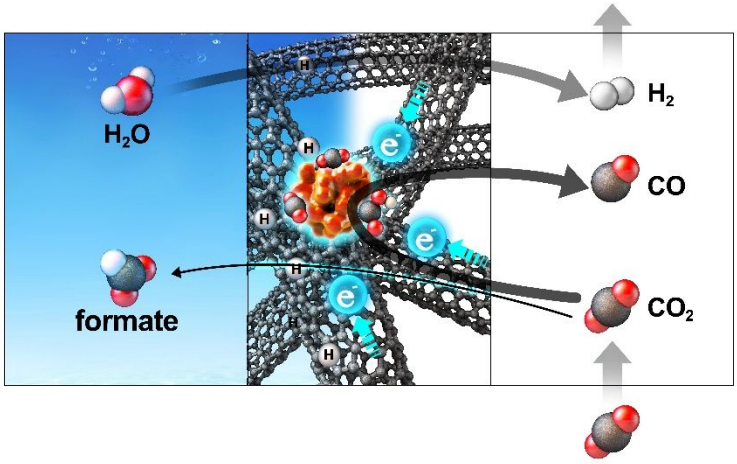

Electrochemical CO_2 reduction has attracted increasing interest as a route to reduce the emission of greenhouse gases, while at the same time generating valuable chemicals. The efficiency of this reaction depends critically on the activity of the catalyst and its selectivity for different products.[1-2] Until now, it has been widely assumed that these properties are solely determined by the binding of intermediates to the active site.[2-6] These binding energies have been thought to carve the product selectivity of transition metal catalysts deeply into stone, e.g. Copper being the only metal that produces up to C_{2+} products, Gold and Silver forming CO and Tin producing formic acid. Although catalyst design has enabled to slightly modify these selectivity rules, the overall trends have prevailed until today.

Recent experimental and theoretical work has shown that the reaction environment represents an additional handle to tune the activity and product selectivity of electrocatalysts.[7-14] For instance, Ringe *et al.* showed the control of the electric double layer field by varying the electrolyte-containing cations as a particularly efficient means.[10] In this work, a stronger interfacial field was observed to increase the selectivity for CO formation on Gold and C_2 formation on Copper, both of which

processes are limited by a field-sensitive reaction step.[8, 10, 13] These insights also open up new strategies for designing catalyst materials or electric devices, as was demonstrated e.g. by the utilization of field-effect transistor setups to directly control the interfacial field.[15] So far, however, a strategic design of catalyst materials based on their interfacial field has not yet been demonstrated.

In this Letter, we demonstrate that the interfacial field can be, indeed, used as an engineering handle to design a highly selective electrocatalyst that inverts a long-standing product selectivity rule. In detail, we carried out electrochemical CO_2 reduction on Sn nanoparticles supported on carbon nanotubes and entangled as cylindrical template,[16] enabling CO_2 transport through gas diffusion and liquid phase modes. We show that the carbon nanotube takes an active role in the reaction by increasing the surface charge density due to its positive work-function. From Density Functional Theory (DFT) calculations, we find this eventually to lead to a significant interfacial field on the Sn active sites which drives the reaction towards CO formation instead of the commonly observed formate. Notably, an almost complete selectivity inversion is observed in contrast to all previously reported Sn catalysts, with formate formation on

Sn being almost completely suppressed and happening only on carbon active sites. These conclusions are supported by experiments with different electrolyte-containing alkali cations, showing the field-dependent CO formation rate to change by unprecedented two orders of magnitude when going from Li^+ to Cs^+, while the formate and H_2 formation rates are almost unchanged. Our work represents the first showcase of how interfacial field-modulation can be used as a concept to design electrocatalysts and highlights the significant impact on product selectivity and electrolyte sensitivity. We expect the conclusions and presented catalyst design concept to be widely applicable to many other electrochemical processes that are driven by field-sensitive reaction steps.

Characterization of the Sn-CHF electrode. Scanning electron microscopy (SEM) images of the prepared Sn-CHF electrode showed randomly entangled CNTs structures and formation of pores on the surface and inside of the fiber (cf. **Figure 1** and **Figure S1** in the Supporting Information). Using backscattered secondary electron (BSE) images, we found the Sn nanoparticles to be successfully incorporated into the CNT matrix. The average size of Sn nanoparticles in the Sn-CHF showed no significant difference depending on the Sn loadings and it ranges from 9.53 nm to 20.15 nm (equivalent volume-based) measured using Image J program[17] (cf. **Figure S2** in the Supporting Information). The prepared Sn-CHF for different loadings were determined from energy dispersive X-ray (EDX) spectroscopy and

thermogravimetric analysis (TGA), as shown in **Figure S1 and S3** in the Supporting Information. The X-ray diffraction (XRD) patterns indicated that the deposited Sn nanoparticles existed as oxide forms (SnO and SnO_2) (cf. **Figure S4a** in the Supporting Information), and the characteristic Raman peaks of CNTs at 1358 cm^{-1} (D band) and 1582 cm^{-1} (G band) in **Figure S4b** in the Supporting Information verified that the original property of CNT was maintained in the Sn-CHF.[18] The X-ray photoelectron spectroscopy (XPS) for deconvolution of C 1s and O 1s spectra (cf. **Figure S5** in the Supporting Information) indicated identical functional groups for the Sn-CHF with different Sn loadings.[19-21] The Sn $3d_{5/2}$ and $3d_{3/2}$ spectra of the Sn-CHF from the high-resolution XPS were indicated at 487.5 eV and 496.5 eV, respectively (cf. **Figure 1h** and **Figure S5** in the Supporting Information), and could be deconvoluted into SnO_x and Sn.[21-22] We note that metal oxides are thermodynamically unstable,[23-25] and SnO_x should be reduced to metallic states under neutral to acidic CO_2 reduction conditions, while under alkaline conditions, oxide phases could coexists.[26] The Brunauer-Emmett-Teller (BET) analysis of the Sn-CHF at different loadings showed mesopores with an average pore size from 13.4 nm to 19.58 nm, and the calculated specific surface area was ranged from 60.83 m^2/g to 86.7 m^2/g (**Table S1** of the Supporting Information). The hierarchically ordered pore structure of Sn-CHF will enable in the future a fine control over the field distribution, retention time and mass transport of species which has been shown to impact the CO_2 reduction activity and product selectivity.[21, 27-28]

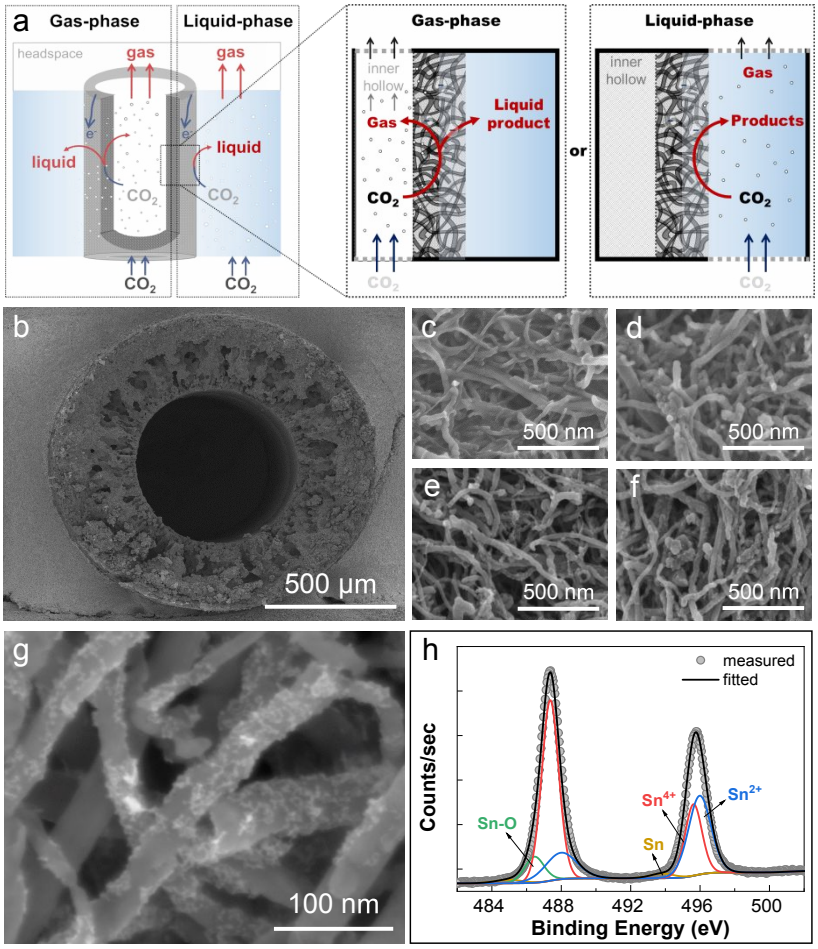

Figure 1. Experimental characterization of the Sn-CHF electrode. (a) Schematic of the hollow-fiber type of gas-diffusion electrode for liquid-phase and gas-phase operation for CO_2RR. (b-g) SEM images of Sn-CHF for cross-sectional image without Sn loading (b), 0 wt.% (c), 5 wt.% (d), 10 wt.% (e), 20 wt.% (f), and using backscattered secondary electron detector for 20 wt.% (g). (h) High-resolution XPS analysis of Sn 3d for 10 wt.% Sn-CHF.

Electrochemical CO_2 reduction. We first tested our electrode in the conventional liquid-phase mode, where CO_2 was provided to the catalyst from the liquid electrolyte outside of the hollow-fiber. Analysis of the Sn-CHF after the reaction indicated no significant physical change of Sn nanoparticles observed from the SEM images (cf. **Figures S6a – S6d** in the Supporting Information). The XPS analysis showed that most of the as-prepared SnO_x on Sn-CHF (cf. **Figure S5** in the Supporting Information) was reduced to metallic Sn^0 under the reaction

condition, indicating that the metallic Sn is most likely the active site (cf. **Figure S6e** in the Supporting Information).

Figure 2 compares the CO/formate product ratio for various previous CO_2R studies on SnO_x-based catalysts (containing no other metal element) with the results from our Sn-CHF catalyst. The analysis shows that previous Sn-based catalysts mainly produce formate, while the Sn-CHF catalyst gives rise to exceptionally high selectivity for CO production (cf. **Figure 2**). In addition, prolonged CO_2 electrolysis using the Sn-CHF with 10 wt.% loading showed stable current density and CO Faradaic efficiency (FE_{CO}) (cf. **Figure S7** in the Supporting Information) during 6 h operation.

Comparison of CO/formate selectivity with previous Sn-based catalysts. The Sn-CHF catalyst is special in the sense that it uses a highly conductive carbon nanotube framework as a support for finely distributed Sn nanoparticles. In search for an explanation for the distinct product selectivity, we first considered the possibility of the Sn oxidation state giving rise to the observed behavior. Previous studies, however, found that oxidized Sn enhanced CO_2R relative to HER,[29-30] but had no effect on the CO vs. formate product selectivity.[29] In addition, a previous study using SnO_x nanoparticles in different oxidation states demonstrated that the production rate for formic acid was enhanced by reducing the nanoparticle size while not affecting CO formation, suggesting instead a role of the local pH at the reaction sites.[31] As detailed below, we further found no CO production from the bare CHF surface (cf. **Figure S8** in the Supporting Information), suggesting that the carbon support does not serve as catalytically active site. Selectivity of CO vs. formate for the Sn-CHF electrode corrected for the activity of the bare CHF (without Sn loading) reached a value of 47 under -0.9 V (*vs.* RHE), where 98% of current for CO_2 reduction was used for CO production.

Analyzing again Figure 2, it can be, however, seen that besides our catalyst, also an N-doped carbon supported Sn catalyst system has been reported with high CO selectivity at low overpotentials, suggesting that the carbon support plays a crucial role.[32] In addition, a strong carbon structure dependence was noted, since various carbon supports such as carbon black,[33] carbon hollow spheres[34] or carbon cloth[27] mainly showed formate selectivity. As further detailed below, we confirmed this structural dependence by carrying out the same experiments in aqueous phase using planar electrodes (activated carbon and CNT powder) which showed preferably formate selectivity (cf. **Figure S9** in the Supporting Information). We thus conclude that the reason for the extraordinary CO selectivity of the Sn-CHF must be seen in advantageous electronic properties of the carbon support, the direct interplay of the carbon material and Sn nanoparticles, and the correspondingly created distinct reaction kinetics and mass transport properties.

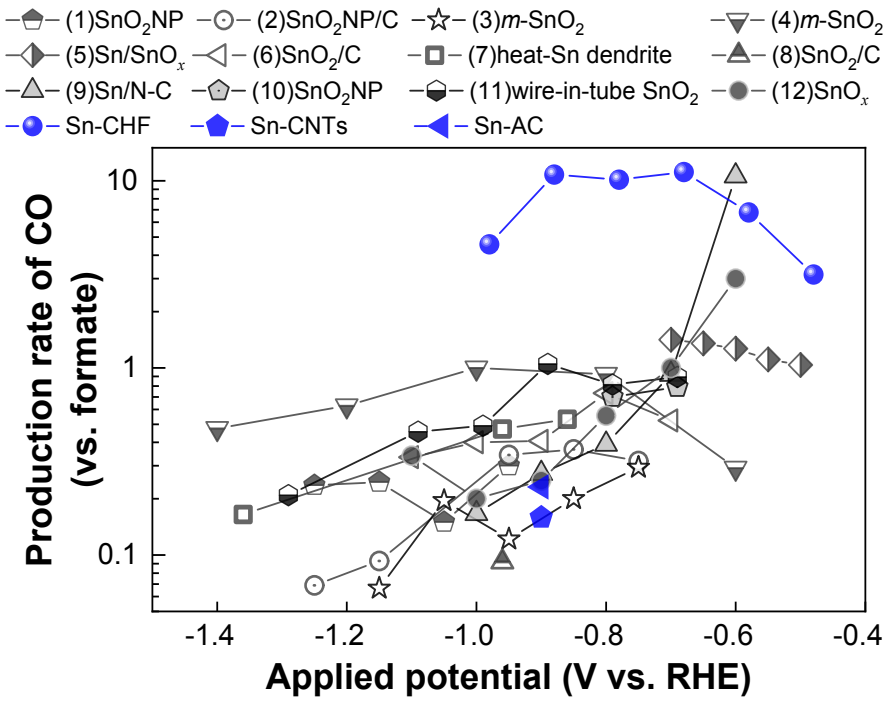

Figure 2. Comparison of selectivity for CO_2R activity with literatures of Sn-based electrodes. The product selectivity for Sn-based CO_2R catalysts is provided as a

function of potential. The Sn-CHF, Sn-CNTs, and Sn-AC with 10 wt.% of Sn loading was tested with 0.1 M $KHCO_3$ and compared with the results from previous studies; (1)-(3),[33] (4),[21] (5),[29] (6),[34] (7),[35] (8),[27] (9),[32] (10)-(11),[22] (12).[6] All data were provided in Table S2 in Supporting Information.

Electric field driven CO formation. Unfunctionalized carbon nanotubes exhibit a high work function of around 5.0 eV,[36] compared to the value of 4.42 eV for Sn.[37] To unravel the implications of this difference under electrochemical conditions, we performed OCP measurements on a bare Sn and the Sn-CHF electrode. As shown in **Figure S10** in the Supporting Information, we found the work function difference to yield a significantly increased OCP of the Sn-CHF electrode of 0.32 V regardless of the amount of Sn loadings compared to -0.40 V for the Sn electrode. The difference of OCP values, that is *ca.* 0.7 V, indeed compares well with the difference of work function, that is *ca.* 0.6 eV. This implies that the Fermi level of the Sn-CHF is dominantly determined by the CNT that consists of the large part of the electrode.

In the absence of faradaic reactions, changes in the OCP directly correlate with changes in the potential of zero charge (PZC) which is related to the electrode surface charge density σ in the constant capacitance regime via:

$$\sigma = C_{\mathrm{dl}} \cdot (U - U^{\mathrm{PZC}}) \#(\text{Equation 1})$$

where C_{dl} is the double layer capacitance, U the electrode potential, and U^{PZC} the PZC. Considering that Sn has a PZC of -0.39 V vs. SHE,[38] a Sn electrode is negatively charged under electrochemical CO_2 reduction conditions. The positive shift of U^{PZC} induced by the CNT

support of the Sn-CHF system builds up more negative charges at the electrode with the same U, as seen from Eq. (1).

Previous studies have shown that the increased surface charge gives rise to an enhanced electric double layer field, which interacts with dipolar reaction intermediates.[8, 10-11, 14, 39-41] We thus carried out surface charge density dependent density functional theory (DFT) calculations on β-Sn(310) on key reaction intermediates that have been discussed in the literature (cf. **Figure 3 a and b**, and **Figure S11 and S12** in the Supporting Information). **Figure 3a** shows the significant stabilization of the $*CO_2$ and *COOH states which have been frequently discussed to limit the rate of CO production e.g. on gold,[8, 42] copper,[10, 43] or silver.[10, 39, 44] In this mechanism (cf. **Figure 3b**), CO_2 adsorption can be limiting or the coupled proton-electron transfer to *COOH, but both reaction steps are enhanced by a more negative surface charge. The increased negative surface charge that we find for the Sn-CHF electrode compared to bare Sn is thus likely an important reason for the enhanced CO production.

In contrast to CO formation, the mechanism for formate production has been controversially discussed. From a general chemical point of view, the C-atom of the adsorbed $*CO_2$ or *COOH is less nucleophilic than the respective O atoms and in combination with the low steric accessibility difficult to be protonated. Due to this, a common assumption has been that formate must be produced via the surface O-bound *OCHO intermediate with the C atom pointing towards the electrolyte solution. A current thermodynamic analysis, however, suggested that the *OCHO intermediate is generally not a good descriptor for the experimentally observed CO vs. formate selectivity trends on transition metals.[4] Instead, the authors showed the *H adsorption energy to separate catalysts in their selectivity for CO vs. formate selectivity and thus be a much more relevant descriptor. In agreement with this argument, *ab initio* molecular dynamics (AIMD) simulations on copper found a high barrier from $*CO_2$ to *OCHO and

suggested formate production to happen via dissolved CO_2 reacting directly with surface-bound *H (cf. **Figure 3b**).[43] In our calculations, we also considered an O-bound *OCO intermediate which could exhibit a smaller kinetic barrier to *OCHO, but found it not to be stable at any applied surface charge. Experiments on boron-doped diamond electrodes also found evidence for formate not being produced via a surface bound *CO_2 intermediate, but via direct reaction from the electrolyte.[45] In sum, these results suggest that formate production likely does not happen via adsorbed carbon species, but instead via a direct reaction of a CO_2 molecule with surface-bound *H atoms. We note that although we decided to consider a bare Sn-facet as active site motif, the variance in field-sensitivity of different reaction intermediates has been shown before to be rather metal independent.[10] The here observed trends should thus also approximately hold for the case of oxidized Sn active sites.

In summary, we envision a reaction mechanism for formate formation through electrochemical generation of *H ("Volmer" step) and following reaction of gaseous CO_2 with surface-adsorbed *H. The large experimentally measured Tafel slopes of 140 – 160 mV/dec for formate production further suggest the possibility of the first electron transfer (Volmer step) being limiting[46] (cf. **Figure S13** in the Supporting Information), but we note that overlapping mass transport effects make a definite conclusion difficult. Most importantly, however, both reaction steps depend on the applied surface charge via the only surface-bound intermediate *H. As seen from **Figure 3a**, we find the *H adsorption energy to be independent of the applied surface charge. From this we follow that formate production happens via a field-insensitive rate-limiting step. In contrast to CO formation, the carbon support does thus not alter the rate of formate production, explaining the unprecedented CO vs. formate selectivity of the Sn-CHF electrode. Other formate production pathways via surface-bound carbon species as e.g. the O-bound *OCO intermediate or the recently discussed *OCOOH intermediate (cf. **Figure S12** in

the Supporting Information) would instead be stabilized by the carbon support and enhance the reaction rate, thus contradicting the experimental observations.

Cation effects on CO formation. In order to find further proof for this mechanism, we performed CO_2R experiments using different cation containing electrolytes. Recent studies suggest that cations with smaller hydration radii are more concentrated in the outer Helmholtz plane, giving rise to increased surface charge density at a fixed potential.[10] Cation exchange can be thus be used as a probe for the field-sensitivity of an electrochemical reaction. **Figures 3c and 3d** show the partial current densities of CO and formate for three different cations of Li^+, K^+ and Cs^+ in 0.1 M bicarbonate solutions (cf. **Figure S14** in the Supporting Information). From this, we first noticed unprecedently strong cation effects, with the CO production rate increasing by a factor of 93 from Li^+ to Cs^+, compared to only a factor of 5 in the case of poly-crystalline Ag.[10, 40, 47] The reason is the very positive PZC of our electrode, which leads to much higher cation concentrations and thus also sensitivity for cation exchange.[10] In contrast to CO, the rate of formate production only increases by a factor of 5.9, the HER rate even only by a factor of 2.4 (cf. **Figure S14d** in the Supporting Information). As discussed above, this variance in the cation sensitivity of the different products can be related to a difference in the field-sensitivity of the rate-limiting step: CO is strongly impacted due to the field-dependence of the rate-limiting CO_2 adsorption step, while formate production is not due to the field-insensitivity of *H adsorption. These results provide a further proof for the suggested mechanism and reveal cation exchange as an efficient technique to alter the product selectivity in particular in highly charged electrode systems.

Carbon nanotube substrate effect. As already discussed in the introduction, previous works on carbon supported Sn nanoparticles observed throughout formate selectivity in contrast to our Sn-CHF electrode. We thus decided to further evaluate the role of the carbon substrate

structure and for that purpose the Sn-CHF electrode was pulverized (represented as Sn-CNT) and coated the powder on a glassy carbon electrode. Electrochemical CO_2 electrolysis using this Sn-CNT electrode produced mainly formate, in accordance with previous studies on different carbon materials.[27, 33-34] Additionally, we also tested an activated carbon electrode with 10 wt.% of Sn loading (denoted as Sn-AC), which also showed preferably formate selectivity, however, with considerably more CO than the Sn-CNT electrode (cf. **Figure S9**). From measuring the OCP, we could correlate this increased CO selectivity again with a higher OCP value (403 mV) compared to that of the Sn-CNT electrode (328 mV) (this trend also agrees with that of previously measured PZC values of 0.80 V[48] and 0.20 V[49] for AC and CNT, respectively) in line with our theoretical understanding (cf. **Figure S9**). From these results, we, however, also see that the hollow-fiber electrode exhibits a specifically dramatic enhancement of field-driven reactions. While future studies have to be performed to unravel the origin, we assume that the strong fields could be attributed to the high electric conductivity resulting from a minimization of resistive intersection sites of the CNT's.[50]

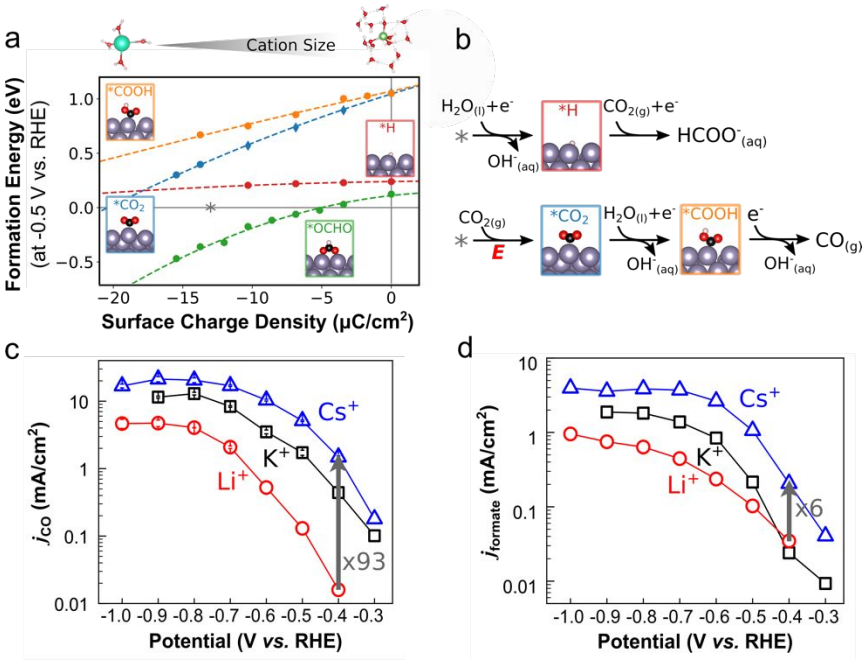

Figure 3. Effects of electrolyte-containing cation exchange. (a) Surface charge dependent formation energies. Formation energies of key reaction intermediates in the CO_2R mechanism are given at -0.5 V vs. RHE and relative to CO_2 and H_2O in the gas phase. (b) Proposed mechanism for CO and formate production. "*E*" indicates a field-sensitive reaction step. (c,d) Polarization curves of CO (c) and formate (d) production with 10 wt.% Sn-CHF in gas-phase reaction at a CO_2 flow rate of 5 sccm using Li^+, K^+ and Cs^+ cations in a 0.1 M bicarbonate solution. The arrow highlights the previously found anti-correlation of the cation size with the surface charge density.[10]

Active sites and intrinsic CO/formate selectivity. The product selectivity of the fabricated Sn-CHF device can be further modulated by changing the mass loading of the Sn nanoparticles. In the liquid phase reaction, we found the CO production rate to correlate with the Sn loading, with no CO formation in the absence of Sn (cf. **Figure 4a**). From this, we conclude that the active sites for CO formation are located on the Sn nanoparticles. In contrast, we recorded formate and H_2 production also from the pure CNT electrode with only slight increases until 10 wt.% Sn loading (cf. **Figure 4a** and **Figure S15** in the Supporting Information). Almost all of the formate, but also most of the H_2, is thus produced from carbon active sites with the Sn nanoparticles only producing minor amounts. This suggests that the product selectivity of Sn, which commonly produces exclusively formate and H_2,[33-35] has been completely switched by the carbon support to 98% intrinsic CO selectivity at -0.9 V (vs. RHE) for 10 wt.% Sn-CHF. This demonstrates the efficiency of the carbon support to generate a strong interfacial field

which eventually inverts the product selectivity as known from previous electrochemical studies. At 20 wt.% Sn loading, the H_2, but in particular the formate partial current density experiences a rapid increase (cf. **Figure 4a** and **Figure S15 e and f** in the Supporting Information). By performing contact angle measurements (cf. **Figure 4b**), we found the increase to correlate with a sudden increase of the hydrophilicity of the electrode. We hypothesize that this critical increase leads to a significant wetting of the electrode exposing a large number of carbon-active sites to the reactants, thus increasing the partial currents in liquid-phase reaction (cf. **Figure 4c**). The interested reader is also referred to the Supporting Information for the dependence of the Sn loading and the CO_2 flow rates in the gas phase operation mode (cf. **Figure S15 – S19** in the Supporting Information).

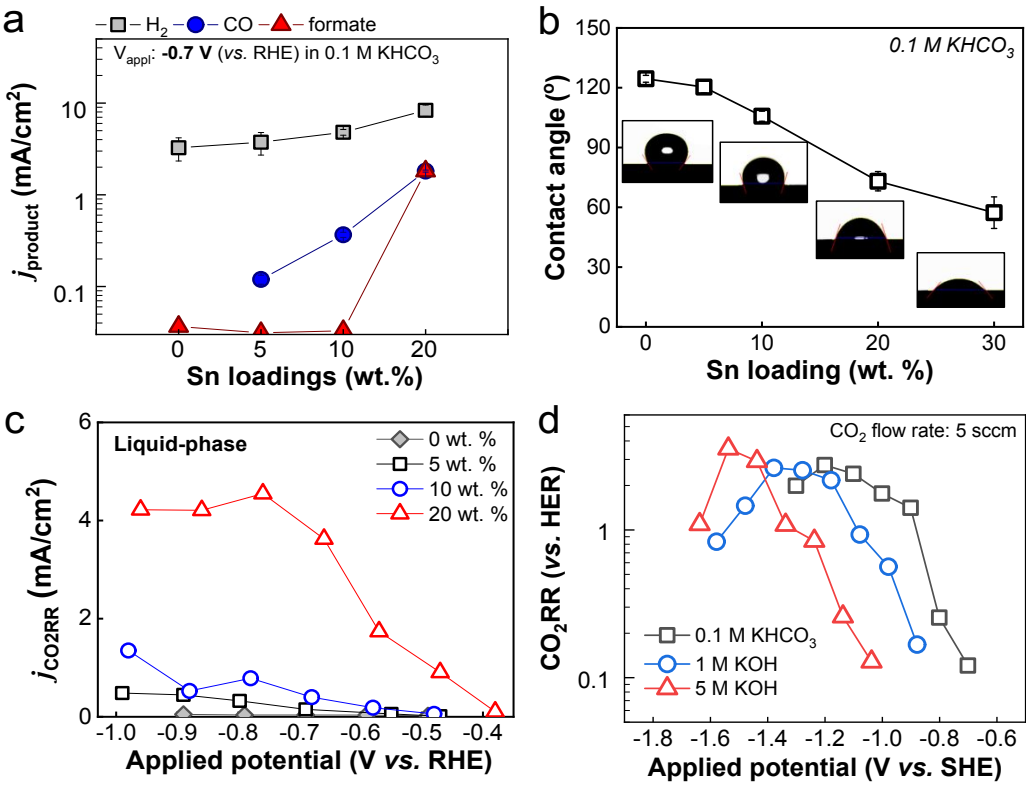

Figure 4. Performances of CO_2R with different experimental conditions. (a) Partial current densities as a function of Sn mass loading at -0.7 V vs. RHE in the liquid-phase

operation mode. (b) Sn mass loading dependent contact angle. (c) CO_2R polarization curve. The current density is given for the liquid-phase operation mode using different Sn mass loadings. (d) pH-dependence of the CO_2R selectivity vs. HER for 10 wt.% Sn-CHF in the gas-phase reaction mode at a CO_2 flow rate of 5 sccm.

Enhancing the CO_2R/HER selectivity using the bulk pH. Finally, we also investigated the influence of the bulk electrolyte pH on the CO_2 reduction activity of the prepared Sn-CHF system (cf. **Figure 4d** and **Figure S20** in the Supporting Information). For this purpose, we performed CO_2R experiments at 10 wt.% Sn loading under the gas diffusion mode at CO_2 flow rate of 5 sccm, for which we obtained the largest selectivity for CO_2R relative to HER. Under the applied alkaline pH conditions, we expect water to be the relevant proton donor. In consequence, all electrochemical reactions that are limited by a proton-transfer should be pH independent on an SHE scale.[8, 51] As a result, we found the HER rate to be nearly unchanged on an SHE scale (cf. **Figure S20d** in the Supporting Information). The CO_2 reduction rate to formate and CO, in contrast, showed a decrease with pH on an SHE scale in the kinetic region of the polarization curve (cf. **Figure S20 b and c** in the Supporting Information). This can be explained by the reduced CO_2 concentration at higher pH values.[52] In consequence, the highest CO_2R products vs. H_2 selectivity can be achieved under the neutral reaction conditions, reaching a production rate ratio of 1.76 at a small applied potential of -1.0 V (*vs*. SHE).

The selectivity and current density for CO production of the Sn-CHF was compared to previous reports of Sn-based catalysts in **Figure S21** of the Supporting Information. The CO selectivity using Sn-CHF was relatively unaffected by the change of operational mode from the liquid-phase to gas-phase, and it showed the highest selectivity versus formate, regardless of

operational conditions among the Sn based electrodes. On the other hand, the Sn-CHF under gas-phase operation indicated considerable increase of j_{CO} as compared to those under the liquid-phase mode.

In summary, we presented a carbon nanotube supported Sn catalyst which showed a complete inversion of the product selectivity on Sn from commonly produced formate to exclusive CO production. We determined the origin for the unusual formation of CO to be due to enhanced charging of the carbon support which effectively charges up the Sn active site environment favoring the field-sensitive reaction pathway to CO. We found that this enhanced charging is likely correlated with the positive PZC of the carbon support, as well as the use of an electrically conductive, almost intersection-free arrangement of the CNTs. From DFT calculations, we found the critical reaction step for CO production to be CO_2 adsorption which is significantly enhanced by the interfacial field. In contrast, formate and H_2 production are almost completely suppressed on the Sn nanoparticles, since they are driven by a field-insensitive reaction step (*H adsorption). We also presented an unprecedentedly high, two orders of magnitude increase of the CO production rate when tuning the electric field by exchange of the electrolyte-containing cations from Li^+ to Cs^+. In contrast, the formate

and H_2 formation rates were nearly unchanged. Finally, we also presented strategies to bring the inexpensive catalyst to an industrially applicable performance scale such as the optimization of mass transport (via a gas diffusion electrode), an increase of the geometric current density (via a large density of carbon nanotubes). Our work can be seen as a pioneering example toward a new era of catalyst design by facilitating surface charge and an interfacial field control. Previous studies, for example, suggested the importance of field-effects in the formation of C_2 products on Copper,[10, 13] which may be enhanced by utilizing similar carbon support materials. Future studies on such systems have to be accompanied by careful control of the charge distribution and interfacial field by designing the catalyst-support arrangements at the nano-scale.

ASSOCIATED CONTENT

Supporting Information.

Detailed methods including synthesis and characterization of Sn-CHF, electrochemical CO_2 reduction, and DFT calculations; figures for SEM images, particle size distributions, TGA, XRD, Raman, XPS, DFT calculations, electrochemical analyses, and comparison of performances reported in the literature (PDF)

AUTHOR INFORMATION

Corresponding Authors

Hyungjun Kim – Department of Chemistry, Korea Advanced Institute of Science and Technology, 291 Daehak-ro, Yuseong-gu, Daejeon 34141, Republic of Korea.

Seoktae Kang – Department of Civil and Environmental Engineering, Korea Advanced Institute of Science and Technology, 291 Daehak-ro, Yuseong-gu, Daejeon 34141, Republic of Korea.

Youngkook Kwon – School of Energy and Chemical Engineering, Ulsan National Institute of Science and Technology, 50 UNIST-gil, Ulsan 44919, Republic of Korea.

Authors

Mi-Young Lee – Department of Civil and Environmental Engineering, Korea Advanced Institute of Science and Technology, 291 Daehak-ro, Yuseong-gu, Daejeon 34141, Republic of Korea.

Stefan Ringe – Department of Energy Science and Engineering, Daegu Gyeongbuk Institute of Science and Technology (DGIST), Daegu 42988, Republic of Korea.

Author Contributions

M.-Y.L. and S.R. contributed equally to this work.

Notes

The authors declare no competing financial interest.

ACKNOWLEDGMENT

This work was supported as part of the ‘‘Next Generation Carbon Upcycling Project’’ (Project No. 2017M1A2A2043150 and No. 2020M1A2A6079127) through the National Research Foundation (NRF) funded by the Ministry of Science and ICT, Republic of Korea. S.R. and H.K. also acknowledge the support by the “Creative Materials Discovery Program” (Project No. 2017M3D1A1039378) through the NRF. Special thanks to Jung-Ae Lim (Environment & Sustainable Resources Research Center, Korea Research Institute of Chemical Technology) for supporting experimental cell design and set-up.

REFERENCES

1. Lu, X.; Wu, Y.; Yuan, X.; Huang, L.; Wu, Z.; Xuan, J.; Wang, Y.; Wang, H., High-Performance Electrochemical CO_2 Reduction Cells Based on Non-noble Metal Catalysts. *ACS Energy Lett.* **2018,** *3* (10), 2527-2532, DOI: 10.1021/acsenergylett.8b01681

2. Ju, W.; Bagger, A.; Wang, X.; Tsai, Y.; Luo, F.; Möller, T.; Wang, H.; Rossmeisl, J.; Varela, A. S.; Strasser, P., Unraveling Mechanistic Reaction Pathways of the

Electrochemical CO_2 Reduction on Fe–N–C Single-Site Catalysts. *ACS Energy Lett.* **2019,** *4* (7), 1663-1671, DOI: 10.1021/acsenergylett.9b01049

3. Hussain, J.; Jónsson, H.; Skúlason, E., Calculations of Product Selectivity in Electrochemical CO_2 Reduction. *ACS Catal.* **2018,** *8* (6), 5240-5249, 10.1021/acscatal.7b03308

4. Bagger, A.; Ju, W.; Varela, A. S.; Strasser, P.; Rossmeisl, J., Electrochemical CO_2 Reduction: A Classification Problem. *ChemPhyschem* **2017,** *18* (22), 3266-3273, DOI: 10.1002/cphc.201700736

5. Kas, R.; Yang, K.; Bohra, D.; Kortlever, R.; Burdyny, T.; Smith, W. A., Electrochemical CO_2 reduction on nanostructured metal electrodes: fact or defect? *Chem. Sci.* **2020,** *11* (7), 1738-1749, DOI: 10.1039/C9SC05375A

6. Cai, Z.; Wu, Y.; Wu, Z.; Yin, L.; Weng, Z.; Zhong, Y.; Xu, W.; Sun, X.; Wang, H., Unlocking Bifunctional Electrocatalytic Activity for CO_2 Reduction Reaction by Win-Win Metal–Oxide Cooperation. *ACS Energy Lett.* **2018,** *3* (11), 2816-2822, DOI: 10.1021/acsenergylett.8b01767

7. Resasco, J.; Chen, L. D.; Clark, E.; Tsai, C.; Hahn, C.; Jaramillo, T. F.; Chan, K.; Bell, A. T., Promoter Effects of Alkali Metal Cations on the Electrochemical Reduction of Carbon Dioxide. *J. Am. Chem. Soc.* **2017,** *139* (32), 11277-11287, DOI: 10.1021/jacs.7b06765

8. Ringe, S.; Morales-Guio, C. G.; Chen, L. D.; Fields, M.; Jaramillo, T. F.; Hahn, C.; Chan, K., Double layer charging driven carbon dioxide adsorption limits the rate of electrochemical carbon dioxide reduction on Gold. *Nat. Commun.* **2020,** *11* (1), 33, DOI: 10.1038/s41467-019-13777-z

9. Liu, M.; Pang, Y.; Zhang, B.; De Luna, P.; Voznyy, O.; Xu, J.; Zheng, X.; Dinh, C. T.; Fan, F.; Cao, C.; et al., Enhanced electrocatalytic CO_2 reduction via field-induced reagent concentration. *Nature* **2016,** *537* (7620), 382-386, DOI: 10.1038/nature19060

10. Ringe, S.; Clark, E. L.; Resasco, J.; Walton, A.; Seger, B.; Bell, A. T.; Chan, K., Understanding cation effects in electrochemical CO_2 reduction. *Energy Environ. Sci.* **2019,** *12* (10), 3001-3014, DOI: 10.1039/C9EE01341E

11. Chen, L. D.; Urushihara, M.; Chan, K.; Nørskov, J. K., Electric Field Effects in Electrochemical CO_2 Reduction. *ACS Catal.* **2016,** *6* (10), 7133-7139, DOI: 10.1021/acscatal.6b02299

12. Zheng, T.; Jiang, K.; Ta, N.; Hu, Y.; Zeng, J.; Liu, J.; Wang, H., Large-Scale and Highly Selective CO_2 Electrocatalytic Reduction on Nickel Single-Atom Catalyst. *Joule* **2019,** *3* (1), 265-278, DOI: 10.1016/j.joule.2018.10.015

13. Sandberg, R. B.; Montoya, J. H.; Chan, K.; Nørskov, J. K., CO-CO coupling on Cu facets: Coverage, strain and field effects. *Surf. Sci.* **2016,** *654*, 56-62, DOI: 10.1016/j.susc.2016.08.006

14. Murata, A.; Hori, Y., Product Selectivity Affected by Cationic Species in Electrochemical Reduction of CO_2 and CO at a Cu Electrode. *Bull. Chem. Soc. Jpn.* **1991,** *64* (1), 123-127, DOI: 10.1246/bcsj.64.123

15. Wu, Y.; Ringe, S.; Wu, C.-L.; Chen, W.; Yang, A.; Chen, H.; Tang, M.; Zhou, G.; Hwang, H. Y.; Chan, K.; et al., A Two-Dimensional MoS_2 Catalysis Transistor by

Solid-State Ion Gating Manipulation and Adjustment (SIGMA). *Nano Lett.* **2019,** *19* (10), 7293-7300, DOI: 10.1021/acs.nanolett.9b02888

16. Lee, M.-Y.; Han, S.; Lim, H.; Kwon, Y.; Kang, S., Electrocatalytic CO_2 Reduction via a Permeable CNT Hollow-Fiber Electrode Incorporated with SnO_2 Nanoparticles. *ACS Sustain. Chem. Eng.* **2019,** *8* (5), 2117-2121, DOI: 10.1021/acssuschemeng.9b05701

17. Schneider, C. A.; Rasband, W. S.; Eliceiri, K. W., NIH Image to ImageJ: 25 years of image analysis. *Nat. Methods* **2012,** *9* (7), 671-675, DOI: 10.1038/nmeth.2089

18. Li, Y.-S.; Liao, J.-L.; Wang, S.-Y.; Chiang, W.-H., Intercalation-assisted longitudinal unzipping of carbon nanotubes for green and scalable synthesis of graphene nanoribbons. *Sci. Rep.* **2016,** *6*, 22755, DOI: 10.1038/srep22755

19. Sun, J.; Xu, J.; Jiang, H.; Zhang, X.; Niu, D., Roles of Oxygen Functional Groups in Carbon Nanotubes-Supported Ag Catalysts for Electrochemical Conversion of CO_2 to CO. *ChemElectroChem* **2020,** *7* (8), 1869-1876, DOI: 10.1002/celc.202000026

20. Zhang, Q.; Zhang, Y.; Mao, J.; Liu, J.; Zhou, Y.; Guay, D.; Qiao, J., Electrochemical Reduction of CO_2 by SnO_x Nanosheets Anchored on Multiwalled Carbon Nanotubes with Tunable Functional Groups. *ChemSusChem* **2019,** *12* (7), 1443-1450, DOI: 10.1002/cssc.201802725

21. Ge, H.; Gu, Z.; Han, P.; Shen, H.; Al-Enizi, A. M.; Zhang, L.; Zheng, G., Mesoporous tin oxide for electrocatalytic CO_2 reduction. *J. Colloid Interf. Sci.* **2018,** *531*, 564-569, DOI: 10.1016/j.jcis.2018.07.066

22. Fan, L.; Xia, Z.; Xu, M.; Lu, Y.; Li, Z., 1D SnO_2 with Wire-in-Tube Architectures for Highly Selective Electrochemical Reduction of CO_2 to C_1 Products. *Adv. Funct. Mater.* **2018,** *28* (17), 1706289, DOI: 10.1002/adfm.201706289

23. Cui, C.; Han, J.; Zhu, X.; Liu, X.; Wang, H.; Mei, D.; Ge, Q., Promotional effect of surface hydroxyls on electrochemical reduction of CO_2 over SnO_x/Sn electrode. *J. Catal.* **2016,** *343*, 257-265, DOI: 10.1016/j.jcat.2015.12.001

24. Jeong, H. M.; Kwon, Y.; Won, J. H.; Lum, Y.; Cheng, M. J.; Kim, K. H.; Head-Gordon, M.; Kang, J. K., Atomic-Scale Spacing between Copper Facets for the

Electrochemical Reduction of Carbon Dioxide. *Adv. Energy Mater.* **2020,** *10* (10), 1903423, DOI: 10.1002/aenm.201903423

25. Baruch, M. F.; Pander, J. E.; White, J. L.; Bocarsly, A. B., Mechanistic Insights into the Reduction of CO_2 on Tin Electrodes using in Situ ATR-IR Spectroscopy. *ACS Catal.* **2015,** *5* (5), 3148-3156, DOI: 10.1021/acscatal.5b00402

26. Awan, I. Z.; Khan, A. Q., Corrosion-Occurrence & Prevention. *J. Chem. Soc. Pak.* **2018,** *40* (4), 602-655.

27. Li, F.; Chen, L.; Knowles, G. P.; MacFarlane, D. R.; Zhang, J., Hierarchical Mesoporous SnO_2 Nanosheets on Carbon Cloth: A Robust and Flexible Electrocatalyst for CO_2 Reduction with High Efficiency and Selectivity. *Angew. Chem. Int. Ed.* **2017,** *56* (2), 505-509, DOI: 10.1002/anie.201608279

28. Karaiskakis, A. N.; Golru, S. S.; Biddinger, E. J., Effect of Electrode Geometry on Selectivity and Activity in CO_2 Electroreduction. *Ind. Eng. Chem. Res.* **2019,** *58* (50), 22506-22515, DOI: 10.1021/acs.iecr.9b03762

29. Chen, Y.; Kanan, M. W., Tin Oxide Dependence of the CO_2 Reduction Efficiency on Tin Electrodes and Enhanced Activity for Tin/Tin Oxide Thin-Film Catalysts. *J. Am. Chem. Soc.* **2012,** *134* (4), 1986-1989, DOI: 10.1021/ja210879

30. Dutta, A.; Kuzume, A.; Rahaman, M.; Vesztergom, S.; Broekmann, P., Monitoring the Chemical State of Catalysts for CO_2 Electroreduction: An In Operando Study. *ACS Catal.* **2015,** *5* (12), 7498-7502, DOI: 10.1021/acscatal.5b02322

31. Gu, J.; Héroguel, F.; Luterbacher, J.; Hu, X., Densely Packed, Ultra Small SnO Nanoparticles for Enhanced Activity and Selectivity in Electrochemical CO_2 Reduction. *Angew. Chem. Int. Ed.* **2018,** *57* (11), 2943-2947, DOI: 10.1002/anie.201713003

32. Zhao, Y.; Liang, J.; Wang, C.; Ma, J.; Wallace, G. G., Tunable and Efficient Tin Modified Nitrogen-Doped Carbon Nanofibers for Electrochemical Reduction of Aqueous Carbon Dioxide. *Adv. Energy Mater.* **2018,** *8* (10), 1702524, DOI: 10.1002/aenm.201702524

33. Daiyan, R.; Lu, X.; Saputera, W. H.; Ng, Y. H.; Amal, R., Highly Selective Reduction of CO_2 to Formate at Low Overpotentials Achieved by a Mesoporous Tin

Oxide Electrocatalyst. *ACS Sustain. Chem. Eng.* **2018,** *6* (2), 1670-1679, DOI: 10.1021/acssuschemeng.7b02913

34. Yiliguma; Wang, Z.; Yang, C.; Guan, A.; Shang, L.; Al-Enizi, A. M.; Zhang, L.; Zheng, G., Sub-5 nm SnO_2 chemically coupled hollow carbon spheres for efficient electrocatalytic CO_2 reduction. *J. Mater. Chem. A* **2018,** *6* (41), 20121-20127, DOI: 10.1039/C8TA08058E

35. Won, D. H.; Choi, C. H.; Chung, J.; Chung, M. W.; Kim, E.-H.; Woo, S. I., Rational Design of a Hierarchical Tin Dendrite Electrode for Efficient Electrochemical Reduction of CO_2. *ChemSusChem* **2015,** *8* (18), 3092-3098, DOI: 10.1002/cssc.201500694

36. Shiraishi, M.; Ata, M., Work function of carbon nanotubes. *Carbon* **2001,** *39* (12), 1913-1917, DOI: 10.1016/S0008-6223(00)00322-5

37. Hölzl, J.; Schulte, F. K.; Wagner, H., *Solid State Physics*. In *Springer Tracts in Modern Physics*, Springer: New York, 1979.

38. Vayenas, Costas G.; White, Ralph E.; Gamboa-Aldeco, Maria E. *Modern Aspects of Electrochemistry*; Springer-Verlag New York, 2008.

39. Clark, E. L.; Ringe, S.; Tang, M.; Walton, A.; Hahn, C.; Jaramillo, T. F.; Chan, K.; Bell, A. T., Influence of Atomic Surface Structure on the Activity of Ag for the Electrochemical Reduction of CO_2 to CO. *ACS Catal.* **2019**, 4006-4014, DOI: 10.1021/acscatal.9b00260

40. Resasco, J.; Chen, L. D.; Clark, E.; Tsai, C.; Hahn, C.; Jaramillo, T. F.; Chan, K.; Bell, A. T., Promoter Effects of Alkali Metal Cations on the Electrochemical Reduction of Carbon Dioxide. *J. Am. Chem. Soc.* **2017,** *139* (32), 11277-11287, DOI: 10.1021/jacs.7b06765

41. Zhao, S.-F.; Horne, M.; Bond, A. M.; Zhang, J., Is the Imidazolium Cation a Unique Promoter for Electrocatalytic Reduction of Carbon Dioxide? *J. Phys. Chem. C* **2016,** *120* (42), 23989-24001, DOI: 10.1021/acs.jpcc.6b08182

42. Dunwell, M.; Luc, W.; Yan, Y.; Jiao, F.; Xu, B., Understanding Surface-Mediated Electrochemical Reactions: CO_2 Reduction and Beyond. *ACS Catal.* **2018,** *8* (9), 8121-8129, DOI: 10.1021/acscatal.8b02181

43. Cheng, T.; Xiao, H.; Goddard, W. A., Reaction Mechanisms for the Electrochemical Reduction of CO_2 to CO and Formate on the Cu(100) Surface at 298K from Quantum Mechanics Free Energy Calculations with Explicit Water. *J. Am. Chem. Soc.* **2016,** *138*, 13802–13805, DOI: 10.1021/jacs.6b08534

44. Singh, M. R.; Goodpaster, J. D.; Weber, A. Z.; Head-Gordon, M.; Bell, A. T., Mechanistic Insights into Electrochemical Reduction of CO_2 over Ag Using Density Functional Theory and Transport Models. *Proc. Natl. Acad. Sci. U. S. A.* **2017,** *114*, E8812–E8821, DOI: 10.1073/pnas.1713164114

45. Tomisaki, M.; Kasahara, S.; Natsui, K.; Ikemiya, N.; Einaga, Y., Switchable Product Selectivity in the Electrochemical Reduction of Carbon Dioxide Using Boron-Doped Diamond Electrodes. *J. Am. Chem. Soc.* **2019,** *141* (18), 7414-7420, DOI: 10.1021/jacs.9b01773

46. Shinagawa, T.; Garcia-Esparza, A. T.; Takanabe, K., Insight on Tafel slopes from a microkinetic analysis of aqueous electrocatalysis for energy conversion. *Sci. Rep.* **2015,** *5* (1), 13801, DOI: 10.1038/srep13801

47. Singh, M. R.; Kwon, Y.; Lum, Y.; Ager, J. W.; Bell, A. T., Hydrolysis of Electrolyte Cations Enhances the Electrochemical Reduction of CO_2 over Ag and Cu. *J. Am. Chem. Soc.* **2016,** *138* (39), 13006-13012, DOI: 10.1021/jacs.6b07612

48. Wu, T.; Wang, G.; Zhan, F.; Dong, Q.; Ren, Q.; Wang, J.; Qiu, J., Surface-treated carbon electrodes with modified potential of zero charge for capacitive deionization. *Water Res.* **2016,** *93*, 30-37, DOI: 10.1016/j.watres.2016.02.004

49. Barisci, J. N.; Wallace, G. G.; Chattopadhyay, D.; Papadimitrakopoulos, F.; Baughman, R. H., Electrochemical Properties of Single-Wall Carbon Nanotube Electrodes. *J. Electrochem. Soc.* **2003,** *150* (9), E409, DOI: 10.1149/1.1593045

50. Mora, A.; Han, F.; Lubineau, G., Estimating and understanding the efficiency of nanoparticles in enhancing the conductivity of carbon nanotube/polymer composites. *Results Phys.* **2018,** *10*, 81-90, DOI: 10.1016/j.rinp.2018.05.019

51. Liu, X.; Schlexer, P.; Xiao, J.; Ji, Y.; Wang, L.; Sandberg, R. B.; Tang, M.; Brown, K. S.; Peng, H.; Ringe, S.; et al., pH effects on the electrochemical reduction of CO_2 towards C_2 products on stepped copper. *Nat. Commun.* **2019,** *10* (1), 32, DOI: 10.1038/s41467-018-07970-9

52. Gupta, N.; Gattrell, M.; MacDougall, B., Calculation for the cathode surface concentrations in the electrochemical reduction of CO_2 in $KHCO_3$ solutions. *J. Appl. Electrochem.* **2006,** *36* (2), 161-172, DOI: 10.1007/s10800-005-9058-y